THE JOURNAL OF BIOLOGICAL CHEMISTRY VOL. 289, NO. 25, pp. 17932–17940, June 20, 2014

Fully Deacetylated Chitooligosaccharides Act as Efficient Glycoside Hydrolase Family 18 Chitinase Inhibitors*[S]

Received for publication, March 11, 2014, and in revised form, April 29, 2014 Published, JBC Papers in Press, May 14, 2014, DOI 10.1074/jbc.M114.564534

Lei Chen[‡1], **Yong Zhou**[§1], **Mingbo Qu**[‡], **Yong Zhao**[¶], **and Qing Yang**[‡2]

From the [‡]*School of Life Science and Biotechnology, Dalian University of Technology, 2 Linggong Road, Dalian, Liaoning 116024, China, the* [§]*School of Software, Dalian University of Technology, Dalian 116620, China, and the* [¶]*Dalian Institute of Chemical Physics, Chinese Academy of Sciences, Dalian 116023, China*

Background: Chitinase inhibitors have potential applications as pesticides, fungicides, and antiasthmatics.
Results: Fully deacetylated chitooligosaccharides were determined to be GH18 chitinase inhibitors by thermodynamics and crystallography.
Conclusion: Crystal structures reveal a competitive inhibition mode.
Significance: This work first reports fully deacetylated chitooligosaccharides acting as chitinase inhibitors, perhaps providing a structural basis for developing eco-friendly inhibitors against chitinases.

Small molecule inhibitors against chitinases have potential applications as pesticides, fungicides, and antiasthmatics. Here, we report that a series of fully deacetylated chitooligosaccharides $(GlcN)_{2-7}$ can act as inhibitors against the insect chitinase *Of*ChtI, the human chitinase *Hs*Cht, and the bacterial chitinases *Sm*ChiA and *Sm*ChiB with IC_{50} values at micromolar to millimolar levels. The injection of mixed $(GlcN)_{2-7}$ into the fifth instar larvae of the insect *Ostrinia furnacalis* resulted in 85% of the larvae being arrested at the larval stage and death after 10 days, also suggesting that $(GlcN)_{2-7}$ might inhibit *Of*ChtI *in vivo*. Crystal structures of the catalytic domain of *Of*ChtI (*Of*ChtI-CAD) complexed with $(GlcN)_{5,6}$ were obtained at resolutions of 2.0 Å. These structures, together with mutagenesis and thermodynamic analysis, suggested that the inhibition was strongly related to the interaction between the −1 GlcN residue of the inhibitor and the catalytic Glu^{148} of the enzyme. Structure-based comparison showed that the fully deacetylated chitooligosaccharides mimic the substrate chitooligosaccharides by binding to the active cleft. This work first reports the inhibitory activity and proposed inhibitory mechanism of fully deacetylated chitooligosaccharides. Because the fully deacetylated chitooligosaccharides can be easily derived from chitin, one of the most abundant materials in nature, this work also provides a platform for developing eco-friendly inhibitors against chitinases.

Glycoside hydrolase family 18 (GH18)[3] chitinases (EC 3.2.1.14) catalyze the random hydrolysis of *N*-acetyl-β-D-glucosaminide (1→4)-β-linkages in chitin and chitodextrins, which play important roles in various life processes. For example, the well studied bacterium *Serratia marcescens* contains chitinases to degrade chitin for the purpose of nutrition (1–4). Insects secrete chitinases from epithelial cells to digest chitin during development (5, 6). Although chitin is absent in humans, there are two chitinases, chitotriosidase (*Hs*Cht) and acidic mammalian chitinase, that have been identified. *Hs*Cht is secreted by activated macrophages and most likely plays a role in the innate immune response to bacteria, fungi, and other pathogens (7, 8). Acidic mammalian chitinase is expressed in lung and stomach tissue, and an elevated level of acidic mammalian chitinase is often associated with asthma and allergic response (9, 10).

Small molecules against GH18 chitinases have been reported. Most of these inhibitors resemble the structure of oxazolinium ion intermediates or mimic carbohydrate-protein interactions. The pseudotrisaccharide allosamidin, which was isolated from the *Streptomyces* sp., is the most effective inhibitor, with K_i values at the nanomolar level (11–18). The cyclopentapeptides argifin and argadin, which were isolated from the cultured broths of fungal strains *Gliocladium* sp. FTD-0668 and *Clonostachys* sp. FO-7314, respectively (19–21), have IC_{50} values in the nanomolar to micromolar range (21–25). Other molecules, such as chitobiose and chitotriose thiazolines (26), xanthine derivatives (27), and CI-4 (28, 29), exhibit nanomolar to millimolar level inhibitory activities. Unfortunately, complex synthesis and/or limited availability of the starting materials limit the practical application of most of these potent molecules.

On the other hand, mixed randomly deacetylated chitooligosaccharides with different chain lengths have been reported to inhibit the activity of the bacterial chitinase B from *S. marcescens* (*Sm*ChiB) with IC_{50} values of 15–18 μM (30). This inhibition is easily explained based on the catalytic mechanism.

* This work was supported by National High Technology Research and Development Program of China Grant 2011AA10A204; National Key Project for Basic Research Grant 2010CB126100; National Natural Science Foundation of China Grant 61202252; National Key Technology R&D Program Grant 2011BAE06B05; and Specialized Research Fund for the Doctoral Program of Higher Education of China Grant 20120041120052.
[S] This article contains supplemental Figs. S1 and S2.
The atomic coordinates and structure factors (codes 3WQV and 3WQW) have been deposited in the Protein Data Bank (http://wwpdb.org/).
[1] Both authors contributed equally to this work.
[2] To whom correspondence may be addressed. Tel.: 86-411-84707245; Fax: 86-411-84707245; E-mail: qingyang@dlut.edu.cn.

[3] The abbreviations used are: GH18, glycoside hydrolase family 18; *p*NP, 4-nitrophenolate; ITC, isothermal titration calorimetry; MU, methylumbelliferyl; PDB, Protein Data Bank.

Chitinases catalyze hydrolysis through a substrate-assisted mechanism in which the C2 *N*-acetyl group of the −1 sugar of a substrate is the nucleophile that attacks the C1 carbon (31). The GH18 chitinases contain a diagnostic D*X*D*X*E motif in which the glutamate is the catalytic acid/base. Binding of GlcNAc in the −1 subsite requires considerable distortion and is energetically unfavorable (32, 33). Therefore, if the −1 sugar is deacetylated, it may be energetically favorable to bind a GlcN in the −1 subsite (32). Thus, partially and fully deacetylated chitooligosaccharides (*i.e.* oligosaccharides only composed of β-(1–4)-linked D-glucosamine (GlcN, deacetylated unit)) can be inhibitors of GH18 chitinases. Partially deacetylated chitooligosaccharides can be recognized by chitinase as a substrate at a site with an acetylated GlcNAc. Therefore, the use of fully deacetylated inhibitors would prevent the degradation of the inhibitors by chitinase. In this study, we report the degree of polymerization-dependent inhibitory effects of fully deacetylated chitooligosaccharides with a degree of polymerization of 2–7. X-ray crystallographic analysis of the catalytic domain of the GH18 chitinase *Of*ChtI (*Of*ChtI-CAD) complexed with either $(GlcN)_5$ or $(GlcN)_6$ revealed that the crucial interaction is between the key catalytic residue and the −1 GlcN, which suggests that the inhibition is competitive. This work provides the first structural insight into the interaction of deacetylated chitooligosaccharide inhibitors with a chitinase.

EXPERIMENTAL PROCEDURES

Materials—$(GlcN)_2$–$(GlcN)_7$ were purchased from Qingdao BZ Oligo Biotech Co., Ltd. (Qingdao, China). The purities of the GlcN oligomers, determined by high performance liquid chromatography (HPLC), were 98.3, 98.0, 98.7, 97.3, 97.6, and 97.2% for dimer to heptamer, respectively. The GlcN oligomers were analyzed by mass spectrometry to ensure that no GlcNAc was present in the samples. The mixed $(GlcN)_{2-7}$ was purchased from Dalian GlycoBio Co., Ltd. (Dalian, China). The components were determined by HPLC to contain 6.8% $(GlcN)_2$, 21.2% $(GlcN)_3$, 28.4% $(GlcN)_4$, 21.5% $(GlcN)_5$, 9.0% $(GlcN)_6$, 3.1% $(GlcN)_7$, and 10% minor components, including 0.6% GlcN, 2.5% $(GlcN)_8$, 2.7% $(GlcN)_9$, 2.0% $(GlcN)_{10}$, 1.3% $(GlcN)_{11}$, and 0.9% $(GlcN)_{12}$.

*Recombinant Expression and Purification—Of*ChtI (GenBank™ accession number DQ294305) from *Ostrinia furnacalis* was overexpressed and purified as described previously (34). Briefly, the coding sequence for residues Ala^{19}–Leu^{554} of *Of*ChtI was amplified using PCR, and a C-terminal His_6 affinity tag was introduced. The DNA fragment was ligated into pPIC9 (Invitrogen), and the expression plasmid pPIC9-*Of*ChtI was transformed into *Pichia pastoris* GS115 (Invitrogen) by electroporation. *P. pastoris* cells expressing *Of*ChtI were grown in 200 ml of BMGY medium (2% peptone, 1% yeast extract, 1% glycerol, 1.34% yeast nitrogen, 0.2% biotin, and 100 mM potassium phosphate, pH 6.0) at 30 °C for 24 h, and then the cells were collected and resuspended in 1 liter of fresh BMMY medium (2% peptone, 1% yeast extract, 1% methanol, 1.34% yeast nitrogen, 0.2% biotin, and 100 mM potassium phosphate, pH 6.0). Methanol was added to a final concentration of 1% (v/v) at 24-h intervals as an inducer. After incubation for an additional 72 h, the supernatant was harvested via centrifugation. The supernatant was subjected to ammonium sulfate (70% saturation) precipitation at 4 °C. After the precipitate was dissolved, *Of*ChtI was purified using metal chelating chromatography with a nickel-NTA-Sepharose high performance column (5 ml; GE Healthcare).

A fragment corresponding to human chitotriosidase (*Hs*Cht, GenBank™ accession number NM_003465) residues 22–466 (64–1398 bp) was ligated into the pPIC9 vector using the EcoRI restriction sites. The recombinant *Hs*Cht was overexpressed as a secreted protein from the *P. pastoris* GS115 and purified using metal chelating chromatography.

The genes encoding chitinase A and chitinase B from *S. marcescens* (*Sm*ChiA, GenBank™ accession number Z36294; *Sm*ChiB, GenBank™ accession number Z36295) were amplified from the *S. marcescens* genome, and a C-terminal His_6 affinity tag was introduced. The DNA fragments were ligated into pET28a (Novagen, Madison, WI), and the expression plasmids pET28a–*Sm*ChiA and pET28a–*Sm*ChiB were transformed into *Escherichia coli* BL21 (DE3) (Novagen, Madison, WI). The cells were grown to an optical density (OD) of 1.8 at 600 nm before induction with 0.05 mM isopropyl 1-thio-β-D-galactopyranoside. After the addition of isopropyl 1-thio-β-D-galactopyranoside, the growth of cells was continued for 20 h at 16 °C. The target proteins were purified using metal chelating chromatography. The purity of these proteins was analyzed by SDS-PAGE and found to be >95% in all cases.

Site-directed Mutagenesis—The *Of*ChtI E148Q, Y37A, N305A, F309A, and W372A mutants were constructed using the QuikChange site-directed mutagenesis kit (Stratagene, La Jolla, CA) according to the manufacturer's instructions. The mutated genes were sequenced to confirm that the desired mutations were present. The mutants were overexpressed and purified using the same procedure as for wild-type *Of*ChtI.

Enzymatic Assay—Chitinase activities for *Of*ChtI and its mutants, *Hs*Cht, *Sm*ChiA, and *Sm*ChiB, were determined using the chromogenic substrate 4-nitrophenyl β-D-*N*,*N*′-diacetylchitobioside (*p*NP-$(GlcNAc)_2$; Sigma) in a standard assay. In a final volume of 60 μl, 50 nM enzyme was incubated with 0.1 mM substrate *p*NP-$(GlcNAc)_2$ in 20 mM Tris-HCl, pH 7.0, at 30 °C. After the addition of 60 μl of 0.5 M sodium carbonate, the amount of 4-nitrophenylate released was determined by the absorbance at 405 nm. IC_{50} values of fully deacetylated chitooligosaccharides, $(GlcN)_{2-7}$, were determined in the presence of different concentrations of inhibitor. For *Sm*ChiA and *Sm*ChiB, the K_m values for *p*NP-$(GlcNAc)_2$ were determined with increasing concentrations of the substrate from 0.02 to 0.5 mM, and the K_i values for $(GlcN)_{5,6}$ were determined with concentrations of the substrate from 0.075 to 0.3 mM.

The IC_{50} value of $(GlcN)_5$ against *Sm*ChiB was also determined with 4-methylumbelliferyl β-D-*N*,*N*′-diacetylchitobioside (MU-$(GlcNAc)_2$; Sigma) as substrate. Standard reaction mixtures (60 μl) contained 2.5 nM *Sm*ChiB, 20 μM MU-$(GlcNAc)_2$ in 20 mM Tris-HCl, pH 7.0, at 37 °C. The reaction was stopped with 60 μl of 1 M glycine/NaOH (pH 10.6). The released product, MU, was measured by a fluorescence microplate reader (Thermo Fisher Scientific, Waltham, MA) with excitation and emission wavelengths of 360 and 460 nm, respectively.

Isothermal Titration Calorimetry (ITC)—Isothermal titration calorimetry experiments were performed at 25 and 30 °C using a MicroCal iTC$_{200}$ system (Microcal, Northampton, MA). For the experiments with (GlcN)$_{2-7}$, *Of*ChtI, at a concentration of 0.1–0.14 mM in 50 mM HEPES buffer, pH 8.0, was placed in the reaction cell with a volume of 202 μl, and (GlcN)$_{2-7}$, at a concentration of 0.75–4.2 mM in 50 mM HEPES buffer, pH 8.0, was placed in the ITC syringe. Aliquots of 2–3 μl from the syringe were injected into the reaction cell at 120-s intervals with a stirring speed of 1000 rpm. The titrations were typically finished after 13 or 20 injections. The background was measured by injecting the inhibitors into the buffer.

The ITC data collected were processed by the MicroCal Origin version 7.0 software accompanying the ITC$_{200}$ system. Before further analysis, all of the data were corrected for heat of dilution by subtracting the background. Using a nonlinear least squares algorithm in the Origin software, the data were analyzed using a single-site binding model. Using this binding model, the stoichiometry (n), the association constant (K_a), and the binding enthalpy change (ΔH) of the reaction were obtained. For (GlcN)$_2$ and (GlcN)$_3$ binding, a two-site binding model was used. The dissociation constant (K_d), the reaction free energy change (ΔG), and the binding entropy change ($-T\Delta S$) were calculated from the equation,

$$\Delta G = -RT\ln K_a = RT\ln K_d = \Delta H - T\Delta S \qquad \text{(Eq. 1)}$$

where R represents the gas constant (1.98 cal K^{-1} mol^{-1}) and T is the absolute temperature in Kelvin (K).

Crystallization and Data Collection—The crystals of free *Of*ChtI-CAD were obtained in 100 mM HEPES, pH 7.5, 25% (w/v) PEG 3350 by the vapor method as described previously (33). Crystals of the *Of*ChtI-CAD·(GlcN)$_5$ and *Of*ChtI-CAD·(GlcN)$_6$ complexes were obtained by transferring the crystals of free *Of*ChtI-CAD to a solution consisting of 10 mM (GlcN)$_5$ or (GlcN)$_6$, 100 mM HEPES, pH 7.5, 25% (w/v) PEG 3350. These crystals were soaked for 20 h at 4 °C. Afterward, the crystals were soaked for 10 s in a reservoir solution containing 25% (v/v) glycerol as a cryoprotection reagent and subsequently flash-cooled in liquid nitrogen. X-ray diffraction data of the complexes were collected on the BL-17U at the Shanghai Synchrotron Radiation Facility in China. The diffraction data of the complexes were processed using the *HKL*-2000 package (35).

Structure Determination and Refinement—The structures of *Of*ChtI-CAD complexed with (GlcN)$_5$ and (GlcN)$_6$ were solved by molecular replacement with *Phaser* (36) using the structure of free *Of*ChtI-CAD as a model (PDB entry 3W4R). The *PHENIX* suite of programs (37) was used for structure refinement. *Coot* (38) was used for manually building and extending the molecular models. The stereochemical quality of the models was checked by *PROCHECK* (39). The coordinates of *Of*ChtI-CAD with (GlcN)$_5$ and *Of*ChtI-CAD with (GlcN)$_6$ were deposited in the Protein Data Bank as entries 3WQV and 3WQW, respectively. The structural figures were generated using PyMOL (40). The statistics for the diffraction data and the structure refinement are summarized in Table 1.

In Vivo Bioevaluation by Injection of Mixed (GlcN)$_{2-7}$ into the Insect O. furnacalis—*O. furnacalis* larvae were reared using an artificial diet under a photo period of 16 h light and 8 h darkness and a relative humidity of 70–90% at 26–28 °C as described previously (41). In the experimental group, 100 μg of mixed (GlcN)$_{2-7}$ that was dissolved in 2 μl of distilled water was injected into the penultimate abdominal segment of the fifth instar day 5 larvae using a microsyringe. In the control group, 2 μl of distilled water was injected instead. Each group contained 20 individual larvae with three independent replicates. After injection, all of the treated larvae were reared under identical conditions as described above. Mortality and developmental defects were recorded every day before eclosion.

TABLE 1
X-ray data collection and structure refinement statistics

	*Of*ChtI-CAD·(GlcN)$_5$	*Of*ChtI-CAD·(GlcN)$_6$
Space group	P65	P65
Unit cell parameters		
$a = b$ (Å)	94.222	94.219
c (Å)	122.43	122.366
Wavelength (Å)	0.97869	0.97930
Temperature (K)	100	100
Resolution (Å)	50–2.04 (2.08–2.04)	50–2.0 (2.03–2.0)
Unique reflections	39,003	41,613
Observed reflections	38,955	41,593
R_{merge}	0.1 (0.37)	0.11 (0.231)
Average multiplicity	17.1 (17.1)	13.9 (13.9)
$\langle I/\sigma(I)\rangle$	24.08 (11.76)	18.67 (8.98)
Completeness (%)	99 (100)	100 (100)
R/R_{free}	0.1495/0.1676	0.1298/0.1572
Protein atoms	3086	3080
Water molecules	430	490
Other atoms	99	99
Root mean square deviation from ideal		
Bond lengths (Å)	0.004	0.019
Bond angles (degrees)	0.87	1.66
Wilson B factor (Å^2)	21.74	22.68
Average B factor (Å^2)	33.40	24.8
Protein atoms	30.70	21.8
Water molecules	48.40	39.1
Ramachandran plot (%)		
Favored	93.9	93.6
Allowed	6.1	6.4
Outliers	0	0
PDB entry	3WQV	3WQW

RESULTS

Inhibitory Activities—To determine the inhibitory activities of GlcN oligomers against GH18 chitinases, the IC$_{50}$ values of (GlcN)$_{2-7}$ were evaluated by using *p*NP-(GlcNAc)$_2$ as the substrate. Four GH18 chitinases from three different species were tested. They were the insect chitinase *Of*ChtI, the human chitinase *Hs*Cht, and the bacterial chitinases *Sm*ChiA and *Sm*ChiB. The two bacterial enzymes, *Sm*ChiA and *Sm*ChiB, were selected due to their different hydrolysis directions; *Sm*ChiA degrades chitin from its reducing end, whereas *Sm*ChiB degrades chitin from the non-reducing end (42). As shown in Table 2, (GlcN)$_{2-7}$ inhibited the enzymatic activities of the four chitinases with IC$_{50}$ values ranging from 10^1 to 10^3 μM.

For *Of*ChtI, (GlcN)$_2$ was the weakest inhibitor. (GlcN)$_{3-4}$ were moderate inhibitors, and (GlcN)$_{5-7}$ were the most efficient inhibitors. By comparing the IC$_{50}$ values of (GlcN)$_2$, (GlcN)$_3$, and (GlcN)$_4$, we found that the addition of one GlcN residue was accompanied by a 3–4-fold decrease in IC$_{50}$ values. However, if comparing the IC$_{50}$ values of (GlcN)$_4$ and (GlcN)$_5$, the IC$_{50}$ value was decreased by more than 12-fold with the addition of one GlcN residue.

TABLE 2
IC_{50} (μM) of $(GlcN)_{2-7}$ toward four chitinases and three mutants of *Of*ChtI at 30 °C (pH 7.0)

	IC_{50}					
	$(GlcN)_2$	$(GlcN)_3$	$(GlcN)_4$	$(GlcN)_5$	$(GlcN)_6$	$(GlcN)_7$
				μM		
*Of*ChtI[a]						
Wild type	2375.5 ± 433.6	776.0 ± 95.2	204.2 ± 17.3	16.5 ± 2.2	14.5 ± 1.8	11.4 ± 2.1
N305A	2117.1 ± 521.7	802.5 ± 107.2	225.7 ± 23.7	17.1 ± 2.9	15.0 ± 2.5	11.9 ± 1.7
Y37A	2402.2 ± 415.5	787.4 ± 95.2	375.6 ± 28.6	157.3 ± 11.8	151.5 ± 19.7	104.0 ± 13.2
W372A[b]						
F309A	6671.9 ± 496.0	2284.5 ± 242.9	778.1 ± 39.3	68.4 ± 4.7	58.0 ± 2.8	53.3 ± 3.7
*Hs*Cht[a]	3422.5 ± 744.1	1610.0 ± 176.7	637.4 ± 115.6	163.1 ± 19.9	69.5 ± 10.1	37.8 ± 8.6
*Sm*ChiA[a,c]	4125.3 ± 720.9	1700.2 ± 205.3	659.7 ± 98.9	356.4 ± 47.1 (320.7 ± 35.8)[d]	169.7 ± 21.3 (145.5 ± 18.3)[d]	168.0 ± 28.4
*Sm*ChiB[a,c,e]	2997.5 ± 352.6	560.3 ± 114.4	298.8 ± 36.7	116.4 ± 15.4 (89.3 ± 4.2)[d]	72.8 ± 8.6 (52.4 ± 5.8)[d]	65.7 ± 10.1

[a] The IC_{50} values of $(GlcN)_{2-7}$ toward four chitinases were determined with a substrate concentration of 0.1 mM.
[b] W372A showed no activity against *p*NP-$(GlcNAc)_2$.
[c] The K_m values for the substrate *p*NP-$(GlcNAc)_2$ for *Sm*ChiA and *Sm*ChiB were determined by using Lineweaver-Burk plots. The K^m value is 734.1 ± 33.8 μM for *Sm*ChiA and 320.2 ± 28.5 μM for *Sm*ChiB. The substrate concentrations used were 0.02–0.5 mM.
[d] The K_i values for $(GlcN)_5$ and $(GlcN)_6$ for *Sm*ChiA and *Sm*ChiB were determined by using Dixon plots (supplemental Fig. S2). The substrate concentrations used were 0.075–0.3 mM.
[e] The IC_{50} value of $(GlcN)_5$ toward *Sm*ChiB with MU-$(GlcNAc)_2$ as substrate is 127.6 ± 11.9 μM.

For *Hs*Cht, a steady decrease in IC_{50} values by ~2-fold was found to correspond to each increase in the polymerization degree of GlcN (from $(GlcN)_2$ to $(GlcN)_7$). Both $(GlcN)_2$ and $(GlcN)_3$ had IC_{50} values at the 10^3 μM level, which suggested that they were less active. The $(GlcN)_6$ and $(GlcN)_7$ were the most active inhibitors against *Hs*Cht. However, these two GlcN oligomers were 3–4 times less active against *Hs*Cht than toward *Of*ChtI.

For *Sm*ChiA, $(GlcN)_{2-7}$ were poor inhibitors, with the highest IC_{50} value at the 10^2 μM level. For *Sm*ChiB, $(GlcN)_{2-7}$ acted in a similar manner as they did toward *Of*ChtI. The obvious difference was that $(GlcN)_5$, $(GlcN)_6$, and $(GlcN)_7$ exhibited 5–7-fold higher activity against *Of*ChtI than against *Sm*ChiB. From these findings, we concluded that the fully deacetylated chitooligosaccharides $(GlcN)_{2-7}$ are active molecules against chitinases, among which the insect chitinase *Of*ChtI is the most susceptible enzyme.

In Vivo Bioevaluation—To test the *in vivo* efficacy of the fully deacetylated chitooligosaccharides, the mixed $(GlcN)_{2-7}$ were injected into the larvae of the insect *O. furnacalis* at the larval-pupal transition stage, in which *Of*ChtI plays an essential role. As shown in Fig. 1, 3 days after injection, 87% of water-injected larvae pupated, whereas only 15% of the mixed $(GlcN)_{2-7}$-injected larvae pupated. Interestingly, 60% of the $(GlcN)_{2-7}$-injected larvae died at the prepupal stage. Ten days after injection, all of the water-injected individuals completed adult eclosion, whereas 25% of the $(GlcN)_{2-7}$-injected larvae died at the larval stage, and only 15% of the $(GlcN)_{2-7}$-injected individuals completed adult eclosion.

As shown in Fig. 1, 25% of the $(GlcN)_{2-7}$-injected larvae died with their body shrunk seriously. The deaths of the 60% of the $(GlcN)_{2-7}$-injected larvae that molted to prepupal stage appeared to be caused by a failure to shed their old cuticle. For the group that died at the prepupal stage, both the head capsule and the thoracic legs were attached to the body. As observed in Fig. 1, the new pupal cuticle had formed under the old cuticle and tanned underneath. Thus, these larvae died by being trapped in their old cuticles.

Thermodynamics—To investigate the binding of $(GlcN)_{2-7}$ to *Of*ChtI, the thermodynamics of the binding of these inhibitors to *Of*ChtI was determined by using ITC. The binding was assessed in 50 mM HEPES, pH 8.0, at 25 °C. Thermograms and titration curves for $(GlcN)_{2-7}$ are shown in Fig. 2. The derived thermodynamic parameters (n, K_d, ΔG, ΔH, and $-T\Delta S$) are summarized in Table 3.

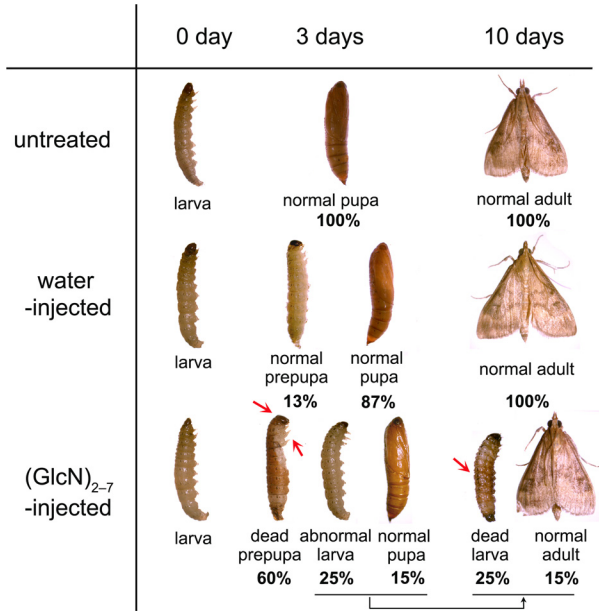

FIGURE 1. **Phenotypes observed after the injection of mixed $(GlcN)_{2-7}$ into the fifth instar day 5 of the insect *O. furnacalis*.** Three days after injection with mixed $(GlcN)_{2-7}$, 60% of the larvae died at the prepupal stage, with the head capsule and the thoracic legs attached to the body (*red arrow*). Ten days after injection with mixed $(GlcN)_{2-7}$, 25% of the larvae died with their body shrunk seriously (*red arrow*). No malformation was found in water-injected control groups.

As shown in Fig. 2, *A* and *B*, the titration curves for $(GlcN)_{2-3}$ fit very well into a two-site binding model with a stoichiometry number of 1.95–1.96. For convenience, we named the site corresponding to K_{d1} the "strong binding site" and the site corresponding to K_{d2} the "weak binding site." $(GlcN)_2$ and $(GlcN)_3$ bound to *Of*ChtI with greater than 1 order of magnitude affinity difference (for $(GlcN)_2$, K_{d1} = 79.4 μM and K_{d2} = 917.2 μM; for $(GlcN)_3$, K_{d1} = 10.2 μM and K_{d2} = 161.1 μM) in the two binding sites. $(GlcN)_3$ bound to *Of*ChtI with ~8-fold and 5-fold higher

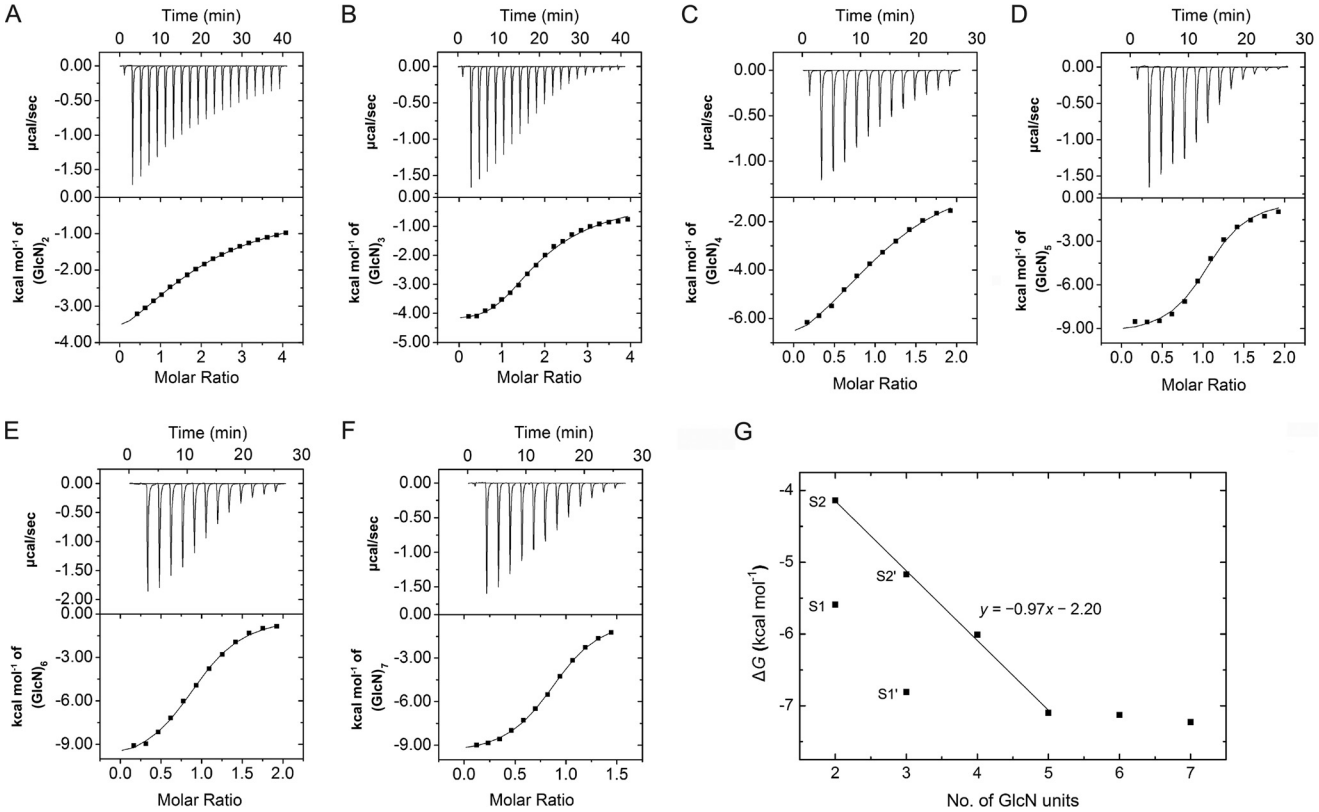

FIGURE 2. *A–F*, thermograms and binding isotherms with theoretical fits for the binding of $(GlcN)_{2-7}$ to *Of*ChtI: $(GlcN)_2$ (*A*), $(GlcN)_3$ (*B*), $(GlcN)_4$ (*C*), $(GlcN)_5$ (*D*), $(GlcN)_6$ (*E*), and $(GlcN)_7$ (*F*). *G*, free energy changes for $(GlcN)_{2-7}$ binding to *Of*ChtI relative to the number of GlcN units in the saccharide chain. $(GlcN)_2$ and $(GlcN)_3$ bind to *Of*ChtI at two sites. For $(GlcN)_2$, S1 is the strong binding site with a low K_d value, and S2 is the weak binding site with a high K_d value. For $(GlcN)_3$, S1′ is the strong binding site with a low K_d value, and S2′ is the weak binding site with a high K_d value.

TABLE 3

Thermodynamic parameters of $(GlcN)_{2-7}$ binding to *Of*ChtI derived from ITC at 25 °C (pH 8.0)

Ligand	n	K_d	ΔG	ΔH	$-T\Delta S$
		μM	*kcal mol^{-1}*	*kcal mol^{-1}*	*kcal mol^{-1}*
$(GlcN)_2$	1.95 ± 0.13	K_{d1}, 79.4 ± 8.7; K_{d2}, 917.2 ± 113.5	ΔG_1, −5.59; ΔG_2, −4.14	ΔH_1, −3.96 ± 0.13; ΔH_2, −13.51 ± 0.86	$-T\Delta S_1$, −1.63; $-T\Delta S_2$, 9.38
$(GlcN)_3$	1.96 ± 0.10	K_{d1}, 10.2 ± 1.6; K_{d2}, 161.1 ± 23.7	ΔG_1, −6.81; ΔG_2, −5.17	ΔH_1, −4.23 ± 0.17; ΔH_2, −7.76 ± 0.31	$-T\Delta S_1$, −2.58; $-T\Delta S_2$, 2.59
$(GlcN)_4$	1.06 ± 0.02	39.2 ± 3.2	−6.01	−9.08 ± 0.10	3.07
$(GlcN)_5$	1.05 ± 0.01	6.2 ± 0.3	−7.10	−9.52 ± 0.24	2.41
$(GlcN)_6$	1.05 ± 0.02	5.9 ± 0.3	−7.13	−9.66 ± 0.09	2.54
$(GlcN)_7$	0.98 ± 0.05	5.0 ± 0.4	−7.23	−10.34 ± 0.42	3.11

affinities than $(GlcN)_2$ at the strong and weak binding sites, respectively. As shown in Table 3, the enthalpy values for $(GlcN)_{2-3}$ at the four sites were negative, which suggested that both strong and weak binding types were exothermic. The two binding processes were enthalpically driven ($|\Delta H| > |-T\Delta S|$). The entropy values ($-T\Delta S_1$) for $(GlcN)_{2-3}$ were greater than zero, which suggested that entropy partly contributed to the strong binding sites of $(GlcN)_{2-3}$.

The titration curves of $(GlcN)_{4-7}$ (Fig. 2, *C–F*) fit the single-site binding model, which suggested the presence of only one binding site. This result, together with the presence of two binding sites for $(GlcN)_{2-3}$, suggested that the long active cleft of *Of*ChtI provides an additional binding site for GlcN oligomers with a low degree of polymerization ($n = 2, 3$). Based on the K_d values of 917.2, 161.1, 39.2, and 6.2 μM for $(GlcN)_2$ at the weak site, $(GlcN)_3$ at the weak site, $(GlcN)_4$, and $(GlcN)_5$, respectively, an increase in the polymerization degree of GlcN by one unit results in a gain in affinity of 4–6-fold. Interestingly, $(GlcN)_4$ exhibited 4-fold weaker binding than $(GlcN)_3$ in the strong binding site. The binding affinities of $(GlcN)_5$, $(GlcN)_6$, and $(GlcN)_7$ to *Of*ChtI were equivalent, which was in agreement with the inhibitory activity data. The enthalpy values were in the range of −9.08 to −10.34 kcal/mol, and entropy values ($-T\Delta S$) were positive, and based on these results, we concluded that the binding of all of the inhibitors examined is exothermic and enthalpically driven. These data suggested that inhibitor binding is accompanied by hydrogen bonding and/or electrostatic-electrostatic interaction.

To analyze the binding free energy changes of these GlcN oligomers, the free energies of $(GlcN)_{2-7}$ binding were plotted against the number of sugar residues (Fig. 2*G*). Interestingly, the binding energies of $(GlcN)_2$ and $(GlcN)_3$ at the weak sites, $(GlcN)_4$, and $(GlcN)_5$ correlated well to the function, $y = -0.97x - 2.20$ (where y represents free energy, and x is the

TABLE 4
Thermodynamic parameters of $(GlcN)_5$ binding to *Of*ChtI and the mutant E148Q derived from ITC at 30 °C (pH 8.0)

Protein	Ligand	n	K_d	ΔG	ΔH	$-T\Delta S$
			μM	*kcal mol*$^{-1}$	*kcal mol*$^{-1}$	*kcal mol*$^{-1}$
*Of*ChtI	$(GlcN)_5$	1.02 ± 0.03	3.9 ± 0.5	−7.48	−11.63 ± 0.34	4.15
E148Q	$(GlcN)_5$	0.91 ± 0.04	73.0 ± 13.2	−5.73	−2.71 ± 0.27	−3.02

number of GlcN residues). Every increase in x (from $(GlcN)_2$ to $(GlcN)_5$) resulted in an average free energy gain of approximately −1.0 kcal mol^{-1}. The free energies of $(GlcN)_6$ and $(GlcN)_7$ binding were equal to the free energy of $(GlcN)_5$ and thus did not fit the model. This result suggested that $(GlcN)_6$ and $(GlcN)_7$ occupied the same number of binding subsites as $(GlcN)_5$.

To investigate the role of the catalytic acid Glu^{148} in inhibitor binding, the mutant E148Q was constructed. The binding of $(GlcN)_5$ to wild-type *Of*ChtI and the mutant E148Q was determined by ITC at 30 °C because of the low heat of $(GlcN)_5$ binding to E148Q at 25 °C. The mutant E148Q bound $(GlcN)_5$ with 19-fold lower affinity than wild-type *Of*ChtI (for *Of*ChtI, K_d = 3.9 μM; for E148Q, K_d = 73.0 μM), as listed in Table 4. The binding of $(GlcN)_5$ to E148Q was entropically driven with an enthalpic contribution ($-T\Delta S$ = −3.02 kcal mol^{-1}, ΔH = −2.71 kcal mol^{-1}), whereas the binding of $(GlcN)_5$ to wild-type *Of*ChtI was strictly enthalpically driven (ΔH = −11.63 kcal mol^{-1}, $-T\Delta S$ = 4.15 kcal mol^{-1}). The reduced binding capacity does not impair ΔG (−1.75 kcal mol^{-1}) very much. However, a dramatic reduction of enthalpic change ($\Delta\Delta H$ = −8.92 kcal mol^{-1}) was observed, which accompanied with a dramatic reduction of entropic change ($\Delta -T\Delta S$ = −7.17 kcal mol^{-1}). This result confirms that a tight interaction is formed between the inhibitors and the catalytic residue Glu^{148}.

Crystallography—To further investigate the inhibitory mechanism of the GlcN oligomers, crystals of *Of*ChtI-CAD were obtained by soaking with the inhibitors $(GlcN)_5$ and $(GlcN)_6$. A nomenclature for sugar-binding subsites was proposed by Davies *et al.* (43), where subsite $+n$ represents the reducing end, subsite $-n$ is the non-reducing end, and the cleavage point is between the −1 and the +1 subsites.

Both of the structures of *Of*ChtI-CAD in complex with $(GlcN)_5$ and $(GlcN)_6$ were solved at a resolution of 2.0 Å. The sixth GlcN residue was surprisingly missing in the *Of*ChtI-CAD·$(GlcN)_6$ complex. The electron density at the +1 subsite could be easily identified as a HEPES molecule, so the missing sixth GlcN residue was not possibly located at the +1 subsite. It is worth noting that some blurry electron density close to the −5 sugar was observed. We thus deduce that the sixth GlcN residue should be the −6 sugar.

The overall structures of *Of*ChtI-CAD·$(GlcN)_5$ and *Of*ChtI-CAD·$(GlcN)_6$ are very similar to the structure of the wild-type enzyme, and all matching atoms had a root mean square deviation of 0.19 Å. Both of the ligands bind to the active cleft (Fig. 3) and could be superposed (Fig. 4*A*). Most of the interactions are between the −1 sugar and the enzyme. As shown in Fig. 3, the pyranose ring of the −1 sugar interacts with the side chain of residue Trp^{372} via a stacking interaction. The O1, O3, and O6 atoms of the −1 sugar form hydrogen bonds with residues Tyr^{217}, Trp^{107}, and Asp^{218}/Arg^{274}, respectively. The C2 amino

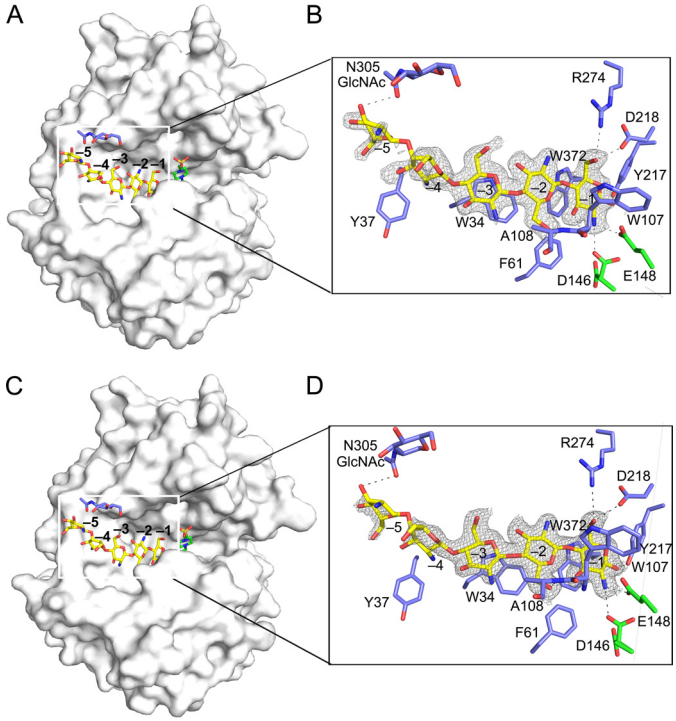

FIGURE 3. **Overall structures of *Of*ChtI-CAD complexed with $(GlcN)_5$ and $(GlcN)_6$.** *A* and *C*, surface representations of *Of*ChtI-CAD complexed with $(GlcN)_5$ (*A*) and $(GlcN)_6$ (*C*). The ligands $(GlcN)_5$ and $(GlcN)_6$, the Asn^{305}-linked *N*-GlcNAc, and the ligand HEPES are shown as *sticks* with *yellow*, *blue*, and *green* carbon atoms, respectively. The *numbers* indicate the subsite to which the GlcN residue is bound. *B* and *D*, details of the active cleft with the interactions between *Of*ChtI-CAD and $(GlcN)_5$ (*B*) or $(GlcN)_6$ (*D*). The ligand is represented as a *stick* with *yellow* carbon atoms, and the $2F_o - F_c$ electron density map around the ligand is contoured at the 2.0σ level. The catalytic residues and the amino acids that interact with the ligand are *labeled* and are shown as *sticks* with *green* and *blue* carbon atoms, respectively. The *numbers* indicate the subsite to which the GlcN residue is bound. Hydrogen bonds between the enzyme and the ligand are drawn as *dashed lines*.

group of the −1 sugar is 2.7 Å from the side chain carboxyl oxygen atoms of the catalytic residues Asp^{146} and Glu^{148}. Compared with the wild-type *Of*ChtI-CAD structure, the side chain of the catalytic Asp^{146} in the *Of*ChtI-CAD·$(GlcN)_5$ structure rotates 91° and faces toward the catalytic Glu^{148}. Additionally, weaker interactions between the −2 to −5 sugars and the enzyme are observed. The O6 atom of the −2 sugar interacts with the amide group of the main chain of residue Ala^{108} through a hydrogen bond. The pyranose ring of the −3 sugar stacks with the aromatic side chain of Trp^{34} via hydrophobic interactions. The glycosidic bond that joins the −3 sugar and the −4 sugar is twisted, which causes the plane of the −4 sugar to lie perpendicular to the planes of the −3, −2, and −1 sugars. The −5 sugar adopts the same orientation as the −4 sugar and is positioned at the end of the substrate-binding cleft. The distance is 3.3 Å between the 3-OH of the −5 GlcN residue and the acetyl oxygen in the GlcNAc conjugated to the glycosylated

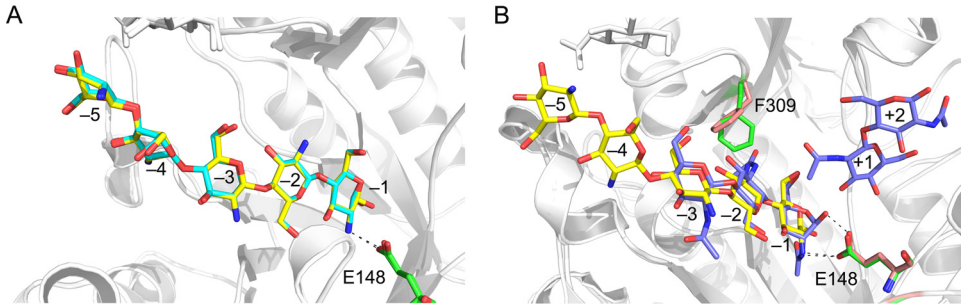

FIGURE 4. *A*, the superposition of the ligands $(GlcN)_5$ and $(GlcN)_6$ in the active cleft of *Of*ChtI-CAD. $(GlcN)_5$ and $(GlcN)_6$ are shown as *sticks* with *yellow* and *cyan* carbon atoms, respectively. The catalytic residue Glu^{148} in two complex structures is *labeled* and shown as *sticks* with *green* carbon atoms. The *numbers* indicate the subsite to which the GlcN residue is bound. Hydrogen bonds between Glu^{148} and the ligands are drawn as a *dashed line*. *B*, superposition of the inhibitor $(GlcN)_5$ and the substrate $(GlcNAc)_{2/3}$ (PDB entry 3WL1) in the substrate-binding cleft of *Of*ChtI-CAD. $(GlcN)_5$ and $(GlcNAc)_{2/3}$ are shown as *sticks* with *yellow* and *blue* carbon atoms, respectively. The catalytic Glu^{148} and Phe^{309} in the structures in complex with $(GlcN)_5$ and $(GlcNAc)_{2/3}$ are *labeled* and shown as *sticks* with *green* and *pink* carbon atoms, respectively. The *numbers* indicate the subsite to which the GlcN and GlcNAc residue is bound. Hydrogen bonds between Glu^{148} and the ligands are drawn as *dashed lines*.

residue Asn^{305}. This is the distance most likely to form a hydrogen bond.

Deduction of the Substrate-binding Subsite −5—The crystal structure of *Of*ChtI-CAD complexed with either $(GlcN)_5$ or $(GlcN)_6$ shows that a hydrogen bond is probably formed between the 3-OH of the −5 GlcN residue and the acetyl oxygen of the glycosylated GlcNAc conjugated to Asn^{305}. Thus, we proposed that this interaction may account for the lower IC_{50} value of $(GlcN)_5$ compared with $(GlcN)_{2-4}$. To verify this hypothesis, Asn^{305} was mutated to Ala^{305}, and the activities of oligosaccharides $(GlcN)_{2-7}$ against the mutant N305A were tested individually. Surprisingly, the mutant N305A was as sensitive as the wild type (Table 2). This result indicated that an interaction was unlikely to take place between the −5 GlcN residue and the glycosylated GlcNAc.

To determine the reason for the 12-fold higher activity of $(GlcN)_5$ compared with $(GlcN)_4$, the structure of a known GH18 chitinase, *Sm*ChiA, was analyzed (44). The structure of SmChiA in complex with $(GlcNAc)_8$ (PDB entry 1EHN) indicates that *Sm*ChiA possesses a substrate binding subsite for the −5 sugar of this substrate. According to the structure-based comparison, *Of*ChtI-CAD is thought to possess a −5 subsite composed of the residue Tyr^{37}. Mutation of Tyr^{37} to Ala^{37} was performed, and inhibitory activities of the oligosaccharides $(GlcN)_{2-7}$ were tested individually. As shown in Table 2, $(GlcN)_2$ and $(GlcN)_3$ exhibited similar effects against both Y37A and the wild-type *Of*ChtI. However, $(GlcN)_4$ and $(GlcN)_{5-7}$ showed 2- and 10-fold weaker inhibitory activity against Y37A than the wild-type enzyme, respectively. Although this was not observed in the crystal structures, we believe that these results suggest that the −5 GlcN is most likely to interact with the aromatic side chain of Tyr^{37} under native conditions.

The mutations along with the inhibitory activity data perhaps suggested the presence of the subsite −5 of *Of*ChtI-CAD. However, further work is needed to verify this assumption.

DISCUSSION

Here we report the inhibitory activities of fully deacetylated chitooligosaccharides. The crystal structures of *Of*ChtI-CAD complexed with the oligomers $(GlcN)_5$ or $(GlcN)_6$ provide structural insights into the inhibitory mechanism.

Inhibitory Mechanism—The crystal structures reveal that the complexed ligand, either $(GlcN)_5$ or $(GlcN)_6$, is located in the binding cleft of *Of*ChtI-CAD at the start of the subsite −1 and interacts with residues that form the cleft wall. A structural comparison of the inhibitor·enzyme complex, *Of*ChtI-CAD·$(GlcN)_5$, with the previously reported substrate·enzyme complex (*Of*ChtI-CAD·$(GlcNAc)_{2/3}$) (PDB entry 3WL1) reveals several differences in the binding modes (Fig. 4*B*).

First, the interactions between the catalytic Glu^{148} residue and the −1 sugar are different (Fig. 4*B*). In the substrate·enzyme complex, the distance is 2.5 Å between the catalytic oxygen of the side chain of Glu^{148} and the C1-OH of the −1 GlcNAc, which suggests that a strong interaction is formed for proton transfer during catalysis. This interaction can be formed if the −1 GlcNAc of the substrate adopts a "boat" conformation. Additionally, the other oxygen of the side chain of Glu^{148} interacts with the C2 acetamido group of the −1 GlcNAc within a distance of 3.0 Å. In the inhibitor·enzyme complex, the catalytic oxygen of Glu^{148} cannot interact with the C1-OH of the −1 GlcN of the inhibitor because the −1 GlcN adopts a "chair" conformation. The only interaction is between the carbonyl oxygen of the side chain of Glu^{148} and the C2 amino group of the −1 GlcN within a distance of 2.5–2.7 Å. This distance is shorter than the distance between Glu^{148} and the C2 acetamido group of the −1 GlcNAc, suggesting that a stronger interaction occurs. The binding of the inhibitor $(GlcN)_5$ to the mutant E148Q exhibited 19-fold lower affinity if compared with the wild type. This result confirms that the catalytic residue Glu^{148} strongly interacts with the inhibitors. Also, the result agrees with the assumption made by Eijsink and co-workers (32) that binding of GlcN in the −1 subsite could be energetically less unfavorable than binding of a GlcNAc.

Second, the comparison indicates that the steric presence of the acetyl group of the −2 GlcNAc has led the Phe^{309} to rotate about 90°, resulting in a farther distance of 3.6 Å between the Phe^{309} and the acetamido group. However, in the enzyme·inhibitor complex, the absence of the *N*-acetyl group lets the Phe^{309} remain still if compared with the unliganded enzyme (PDB code 3W4R). Instead, there is a water-mediated interaction between the residue Arg^{274} and the amino group of the −2 GlcN. It is worth noting that the mutation of the Phe^{309} to Ala^{309} results in only

15% enzymatic activity loss but 4-fold inhibitory activity decrease, perhaps meaning that Phe^{309} is more crucial for the −2 GlcN binding to *Of*ChtI. Taken together, we presume that the lack of an acetyl group at the −2 sugar would facilitate a water molecule to come and to form a water-mediated interaction between the enzyme (Arg^{274}) and the −2 GlcN. Because the Phe^{309} in *Of*ChtI is absent in *Sm*ChiB, we notice that the effect of an acetyl group at the −2 sugar in *Of*ChtI is quite different from that in *Sm*ChiB.

Third, based on the complex structures, both the acetamido group of −3 GlcNAc (in the complex *Of*ChtI·substrate) and the amino group of −3 GlcN (in the complex *Of*ChtI·inhibitor) do not interact directly with the enzyme. However, in both complex structures, a water-mediated interaction is observed. We thus assume that the presence or absence of an acetyl group of the −3 sugar would not harm the binding of a ligand to the enzyme. From the above findings, we conclude that the −1 and −2 subsites are crucial for $(GlcN)_{5,6}$ inhibiting the activity of *Of*ChtI.

$(GlcN)_5$ against SmChiB—The effect of $(GlcN)_5$ against *Sm*ChiB is interesting. Previous studies by Cederkvist *et al.* (30, 45) suggested that the partially deacetylated chitooligosaccharides, perhaps mainly the DADAA (D for GlcN and A for GlcNAc), exhibited a very good inhibitory effect with an IC_{50} value of 16 μM by using the $(GlcNAc)_3$ analog MU-$(GlcNAc)_2$ as substrate. However, in our case, the fully deacetylated chitooligosaccharide, $(GlcN)_5$ (*i.e.* DDDDD according to their nomenclature), exhibited a 8-fold lower inhibitory activity against *Sm*ChiB. Based on the structural information of the *Sm*ChiB·$(GlcNAc)_5$ complex (46), Cederkvist *et al.* concluded that the −2 subsite strongly preferred an acetylated sugar (30). Our result provided a supportive datum to their conclusion.

Structural Differences between Chitinases—It is very surprising that the inhibitory effects of $(GlcN)_{2-7}$ are so different between the chitinases. A structural comparison was then performed. As shown in supplemental Fig. S1, *Of*ChtI possesses an open and the longest hydrophobic cleft, in the middle of which are the +1 and −1 subsites responsible for cleavage occurring. Besides the catalytic site, seven aromatic residues are lined up along the cleft. Among them, four residues, including Trp^{223}, Phe^{194}, Tyr^{243}, and Trp^{241}, follow the +1 subsite, and three residues, including Phe^{61}, Trp^{34}, and Tyr^{37}, follow the −1 subsite. For both *Sm*ChiA and *Hs*Cht, there are two aromatic residues (Phe^{396} and Tyr^{418} in *Sm*ChiA and Trp^{218} and Tyr^{190} in *Hs*Cht) located by the right side of the +1 subsite. However, if compared with the *Sm*ChiA, the *Hs*Cht possesses a wider-ended cleft for binding the non-reducing end of substrates. Unlike *Of*ChtI, *Sm*ChiA, and *Hs*Cht, which possess open clefts, *Sm*ChiB has a blocked cleft with two aromatic residues, Phe^{12} and Phe^{51}, positioned around the −1 subsite. Taken together, we assume that the obvious differences in the architecture of substrate-binding clefts might account for the different effects of $(GlcN)_{2-7}$ between the chitinases.

In summary, we report the polymerization degree-dependent activities of fully deacetylated chitooligosaccharides against chitinases. The crystal structures of the insect chitinase *Of*ChtI complexed with $(GlcN)_{5,6}$ identify a structural explanation for the inhibitory mechanism.

Acknowledgments—We thank Professor Yuguang Du (Dalian Institute of Chemical Physics, Chinese Academy of Science) for kindly providing the fully deacetylated chitooligosaccharides. We thank all of the staff at beamline BL17U of the Shanghai Synchrotron Radiation Facility (China).

REFERENCES

1. Fuchs, R. L., McPherson, S. A., and Drahos, D. J. (1986) Cloning of a *Serratia marcescens* gene encoding chitinase. *Appl. Environ. Microbiol.* **51,** 504–509
2. Jones, J. D., Grady, K. L., Suslow, T. V., and Bedbrook, J. R. (1986) Isolation and characterization of genes encoding two chitinase enzymes from *Serratia marcescens*. *EMBO J.* **5,** 467–473
3. Suzuki, K., Taiyoji, M., Sugawara, N., Nikaidou, N., Henrissat, B., and Watanabe, T. (1999) The third chitinase gene (chiC) of *Serratia marcescens* 2170 and the relationship of its product to other bacterial chitinases. *Biochem. J.* **343,** 587–596
4. Vaaje-Kolstad, G., Horn, S. J., Sørlie, M., and Eijsink, V. G. (2013) The chitinolytic machinery of *Serratia marcescens*: a model system for enzymatic degradation of recalcitrant polysaccharides. *FEBS J.* **280,** 3028–3049
5. Genta, F. A., Blanes, L., Cristofoletti, P. T., do Lago, C. L., Terra, W. R., and Ferreira, C. (2006) Purification, characterization and molecular cloning of the major chitinase from *Tenebrio molitor* larval midgut. *Insect Biochem. Mol. Biol.* **36,** 789–800
6. Fukamizo, T., and Kramer, K. J. (1985) Mechanism of chitin hydrolysis by the binary chitinase system in insect moulting fluid. *Insect Biochem.* **15,** 141–145
7. Barone, R., Simporé, J., Malaguarnera, L., Pignatelli, S., and Musumeci, S. (2003) Plasma chitotriosidase activity in acute *Plasmodium falciparum* malaria. *Clin. Chim. Acta* **331,** 79–85
8. Labadaridis, I., Dimitriou, E., Theodorakis, M., Kafalidis, G., Velegraki, A., and Michelakakis, H. (2005) Chitotriosidase in neonates with fungal and bacterial infections. *Arch. Dis. Child Fetal Neonatal Ed.* **90,** F531–F532
9. Donnelly, L. E., and Barnes, P. J. (2004) Acidic mammalian chitinase: a potential target for asthma therapy. *Trends Pharmacol. Sci.* **25,** 509–511
10. Kawada, M., Hachiya, Y., Arihiro, A., and Mizoguchi, E. (2007) Role of mammalian chitinases in inflammatory conditions. *Keio J. Med.* **56,** 21–27
11. Andersen, O. A., Dixon, M. J., Eggleston, I. M., and van Aalten, D. M. (2005) Natural product family 18 chitinase inhibitors. *Nat. Prod. Rep.* **22,** 563–579
12. Sakuda, S., Isogai, A., Matsumoto, S., and Suzuki, A. (1987) Search for microbial insect growth regulators. II. Allosamidin, a novel insect chitinase inhibitor. *J. Antibiot.* **40,** 296–300
13. Rao, F. V., Houston, D. R., Boot, R. G., Aerts, J. M., Sakuda, S., and van Aalten, D. M. (2003) Crystal structures of allosamidin derivatives in complex with human macrophage chitinase. *J. Biol. Chem.* **278,** 20110–20116
14. Bortone, K., Monzingo, A. F., Ernst, S., and Robertus, J. D. (2002) The structure of an allosamidin complex with the *Coccidioides immitis* chitinase defines a role for a second acid residue in substrate-assisted mechanism. *J. Mol. Biol.* **320,** 293–302
15. Papanikolau, Y., Tavlas, G., Vorgias, C. E., and Petratos, K. (2003) *De novo* purification scheme and crystallization conditions yield high-resolution structures of chitinase A and its complex with the inhibitor allosamidin. *Acta Crystallogr. D Biol. Crystallogr.* **59,** 400–403
16. Vaaje-Kolstad, G., Houston, D. R., Rao, F. V., Peter, M. G., Synstad, B., van Aalten, D. M., and Eijsink, V. G. (2004) Structure of the D142N mutant of the family 18 chitinase ChiB from *Serratia marcescens* and its complex with allosamidin. *Biochim. Biophys. Acta* **1696,** 103–111
17. Cederkvist, F. H., Saua, S. F., Karlsen, V., Sakuda, S., Eijsink, V. G., and Sørlie, M. (2007) Thermodynamic analysis of allosamidin binding to a family 18 chitinase. *Biochemistry* **46,** 12347–12354
18. Sakuda, S., Isogai, A., Matsumoto, S., Suzuki, A., and Koseki, K. (1986) The structure of allosamidin, a novel insect chitinase inhibitor, produced by *Streptomyces* sp. *Tetrahedron Lett.* **27,** 2475–2478
19. Arai, N., Shiomi, K., Iwai, Y., and Omura, S. (2000) Argifin, a new chitinase

inhibitor, produced by *Gliocladium* sp. FTD-0668. II. Isolation, physicochemical properties, and structure elucidation. *J. Antibiot.* **53,** 609–614
20. Omura, S., Arai, N., Yamaguchi, Y., Masuma, R., Iwai, Y., Namikoshi, M., Turberg, A., Kölbl, H., and Shiomi, K. (2000) Argifin, a new chitinase inhibitor, produced by *Gliocladium* sp. FTD-0668. I. Taxonomy, fermentation, and biological activities. *J. Antibiot.* **53,** 603–608
21. Arai, N., Shiomi, K., Yamaguchi, Y., Masuma, R., Iwai, Y., Turberg, A., Kölbl, H., and Omura, S. (2000) Argadin, a new chitinase inhibitor, produced by *Clonostachys* sp. FO-7314. *Chem. Pharm. Bull.* **48,** 1442–1446
22. Rao, F. V., Houston, D. R., Boot, R. G., Aerts, J. M., Hodkinson, M., Adams, D. J., Shiomi, K., Omura, S., and van Aalten, D. M. (2005) Specificity and affinity of natural product cyclopentapeptide inhibitors against *A. fumigatus*, human, and bacterial chitinases. *Chem. Biol.* **12,** 65–76
23. Dixon, M. J., Andersen, O. A., van Aalten, D. M., and Eggleston, I. M. (2005) An efficient synthesis of argifin: a natural product chitinase inhibitor with chemotherapeutic potential. *Bioorg. Med. Chem. Lett.* **15,** 4717–4721
24. Andersen, O. A., Nathubhai, A., Dixon, M. J., Eggleston, I. M., and van Aalten, D. M. (2008) Structure-based dissection of the natural product cyclopentapeptide chitinase inhibitor argifin. *Chem. Biol.* **15,** 295–301
25. Rush, C. L., Schüttelkopf, A. W., Hurtado-Guerrero, R., Blair, D. E., Ibrahim, A. F., Desvergnes, S., Eggleston, I. M., and van Aalten, D. M. (2010) Natural product-guided discovery of a fungal chitinase inhibitor. *Chem. Biol.* **17,** 1275–1281
26. Macdonald, J. M., Tarling, C. A., Taylor, E. J., Dennis, R. J., Myers, D. S., Knapp, S., Davies, G. J., and Withers, S. G. (2010) Chitinase inhibition by chitobiose and chitotriose thiazolines. *Angew. Chem. Int. Ed. Engl.* **49,** 2599–2602
27. Schüttelkopf, A. W., Andersen, O. A., Rao, F. V., Allwood, M., Lloyd, C., Eggleston, I. M., and van Aalten, D. M. (2006) Screening-based discovery and structural dissection of a novel family 18 chitinase inhibitor. *J. Biol. Chem.* **281,** 27278–27285
28. Houston, D. R., Eggleston, I., Synstad, B., Eijsink, V. G., and van Aalten, D. M. (2002) The cyclic dipeptide CI-4 [cyclo-(L-Arg-D-Pro)] inhibits family 18 chitinases by structural mimicry of a reaction intermediate. *Biochem. J.* **368,** 23–27
29. Houston, D. R., Synstad, B., Eijsink, V. G., Stark, M. J., Eggleston, I. M., and van Aalten, D. M. (2004) Structure-based exploration of cyclic dipeptide chitinase inhibitors. *J. Med. Chem.* **47,** 5713–5720
30. Cederkvist, F. H., Parmer, M. P., Vårum, K. M., Eijsink, V. G. H., and Sørlie, M. (2008) Inhibition of a family 18 chitinase by chitooligosaccharides. *Carbohydr. Polym.* **74,** 41–49
31. Tews, I., Terwisscha van Scheltinga, A. C., Perrakis, A., Wilson, K. S., and Dijkstra, B. W. (1997) Substrate-assisted catalysis unifies two families of chitinolytic enzymes. *J. Am. Chem. Soc.* **119,** 7954–7959
32. Aam, B. B., Heggset, E. B., Norberg, A. L., Sørlie, M., Vårum, K. M., and Eijsink, V. G. (2010) Production of chitooligosaccharides and their potential applications in medicine. *Mar. Drugs* **8,** 1482–1517
33. Chen, L., Liu, T., Zhou, Y., Chen, Q., Shen, X., and Yang, Q. (2014) Structural characteristics of an insect group I chitinase, an enzyme indispensable to moulting. *Acta Crystallogr. D Biol. Crystallogr.* **70,** 932–942
34. Wu, Q., Liu, T., and Yang, Q. (2013) Cloning, expression and biocharacterization of *Of*Cht5, the chitinase from the insect *Ostrinia furnacalis*. *Insect Sci.* **20,** 147–157
35. Otwinowski, Z., and Minor, W. (1997) Processing of x-ray diffraction data collected in oscillation mode. *Methods Enzymol.* **276,** 307–326
36. McCoy, A. J., Grosse-Kunstleve, R. W., Adams, P. D., Winn, M. D., Storoni, L. C., and Read, R. J. (2007) Phaser crystallographic software. *J. Appl. Crystallogr.* **40,** 658–674
37. Adams, P. D., Afonine, P. V., Bunkóczi, G., Chen, V. B., Davis, I. W., Echols, N., Headd, J. J., Hung, L. W., Kapral, G. J., Grosse-Kunstleve, R. W., McCoy, A. J., Moriarty, N. W., Oeffner, R., Read, R. J., Richardson, D. C., Richardson, J. S., Terwilliger, T. C., and Zwart, P. H. (2010) PHENIX: a comprehensive Python-based system for macromolecular structure solution. *Acta Crystallogr. D Biol. Crystallogr.* **66,** 213–221
38. Emsley, P., and Cowtan, K. (2004) Coot: model-building tools for molecular graphics. *Acta Crystallogr. D Biol. Crystallogr.* **60,** 2126–2132
39. Laskowski, R. A., MacArthur, M. W., Moss, D. S., and Thornton, J. M. (1993) PROCHECK: a program to check the stereochemical quality of protein structures. *J. Appl. Crystallogr.* **26,** 283–291
40. DeLano, W. L. (2012) *The PyMOL Molecular Graphics System*, version 1.5.0.1, Schroedinger, LLC, New York
41. Qu, M., Liu, T., Yang, J., and Yang, Q. (2011) The gene, expression pattern and subcellular localization of chitin synthase B from the insect *Ostrinia furnacalis*. *Biochem. Biophys. Res. Commun.* **404,** 302–307
42. Hult, E. L., Katouno, F., Uchiyama, T., Watanabe, T., and Sugiyama, J. (2005) Molecular directionality in crystalline β-chitin: hydrolysis by chitinases A and B from *Serratia marcescens* 2170. *Biochem. J.* **388,** 851–856
43. Davies, G. J., Wilson, K. S., and Henrissat, B. (1997) Nomenclature for sugar-binding subsites in glycosyl hydrolases. *Biochem. J.* **321,** 557–559
44. Papanikolau, Y., Prag, G., Tavlas, G., Vorgias, C. E., Oppenheim, A. B., and Petratos, K. (2001) High resolution structural analyses of mutant chitinase A complexes with substrates provide new insight into the mechanism of catalysis. *Biochemistry* **40,** 11338–11343
45. Cederkvist, F. H., Zamfir, A. D., Bahrke, S., Eijsink, V. G., Sørlie, M., Peter-Katalinić, J., and Peter, M. G. (2006) Identification of a high-affinity-binding oligosaccharide by (+) nanoelectrospray quadrupole time-of-flight tandem mass spectrometry of a noncovalent enzyme-ligand complex. *Angew. Chem. Int. Ed. Engl.* **45,** 2429–2434
46. van Aalten, D. M., Komander, D., Synstad, B., Gåseidnes, S., Peter, M. G., and Eijsink, V. G. (2001) Structural insights into the catalytic mechanism of a family 18 exo-chitinase. *Proc. Natl. Acad. Sci. U.S.A.* **98,** 8979–8984